Biomacromolecules

Article

Cite This: Biomacromolecules 2019, 20, 1709−1718

pubs.acs.org/Biomac

Minimal Reconstitution of Membranous Web Induced by a Vesicle−Peptide Sol−Gel Transition

James C. S. Ho,[†,‡] Christoph Steininger,[†,‡,§,∥,¶] Shu Hui Hiew,[†,‡] Min Chul Kim,[†,‡] Erik Reimhult,[§] Ali Miserez,[†,‡,#] NamJoon Cho,[†,‡,⊥] Atul N. Parikh,*[,†,‡,⊗] and Bo Liedberg*[,†,‡]

[†]Centre for Biomimetic Sensor Science, Nanyang Technological University, 50 Nanyang Drive 637553, Singapore

[‡]School of Materials Science and Engineering, Nanyang Technological University, 50 Nanyang Avenue 639798, Singapore

[§]Institute of Biologically Inspired Materials, University of Natural Resources and Life Sciences, 1190 Vienna, Austria

[∥]International Graduate School on Bionanotechnology, University of Natural Resources and Life Sciences, Austrian Institute of Technology and Nanyang Technological University, Giefinggasse 4, 1210 Vienna, Austria

[¶]BioSensor Technologies, AIT-Austrian Institute of Technology GmbH, Giefinggasse 4, 1210 Vienna, Austria

[#]School of Biological Sciences, Nanyang Technological University, 50 Nanyang Drive 637551, Singapore

[⊥]School of Chemical and Biomedical Engineering, Nanyang Technological University, 62 Nanyang Drive 637459, Singapore

[⊗]Departments of Biomedical Engineering and Materials Science & Engineering, University of California, Davis, Davis, California 95616, United States

Supporting Information

ABSTRACT: Positive strand RNA viruses replicate in specialized niches called membranous web within the cytoplasm of host cells. These virus replication organelles sequester viral proteins, RNA, and a variety of host factors within a fluid, amorphous matrix of clusters of endoplasmic reticulum (ER) derived vesicles. They are thought to form by the actions of a nonstructural viral protein NS4B, which remodels the ER and produces dense lipid−protein condensates. Here, we used *in vitro* reconstitution to identify the minimal components and elucidate physical mechanisms driving the web formation. We found that the N-terminal amphipathic domain of NS4B (peptide 4BAH2) and phospholipid vesicles (∼100−200 nm in diameter) were sufficient to produce a gel-like, viscoelastic condensate. This condensate coexists with the surrounding aqueous phase and affords rapid exchange of molecules. Together, it recapitulates the essential properties of the virus-induced membranous web. Our data support a novel phase separation mechanism in which phospholipid vesicles provide a supramolecular template spatially organizing multiple self-associating peptides thereby generating programmable multivalency *de novo* and inducing macroscopic phase separation.

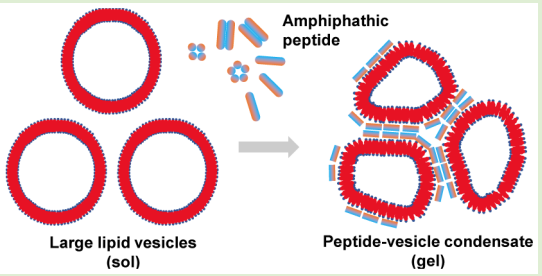

INTRODUCTION

More than a century ago, Edmund B. Wilson advanced the corpuscular conception of the cytoplasm.[1] Reconciling microscopic observations of living protoplasms of eggs of echinoderms, he postulated a complex structure for the cellular interior: a hierarchically organized emulsion of liquids suspended in a continuous fluid substance. The emulsion consists of a dynamic meshwork of a dispersed granular phase or "alveolar bodies" and smaller fluid granules or "microsomes" of well-differentiated chemical compositions. One hundred years later, this mosaic view of the cytoplasm is beginning to re-emerge[2−4] with a twist: the purported roles are reversed. Wilson regarded the granules to be of "*secondary origin and importance*" emphasizing that the protoplasmic activities reside in the continuous background phase. The emerging new view, by contrast, recognizes the colloidal, fluid or gel condensates (membrane-less compartments in space and time, which concentrate some biomolecular components and exclude others) to be functionally relevant both for the normal working and pathophysiology of the living cell. It regards their biogenesis, including the underlying thermodynamic mechanisms of liquid−liquid phase separation (LLPS) and liquid−solid (or fluid-gel) phase transitions[5,6] to represent universal biological strategies for the living cell. These mechanisms enable living cells to dynamically organize the intracellular space and achieve an efficient spatiotemporal control over the diversity of simultaneous, diffusion-limited biochemical reactions inside.

The new condensate hypothesis is gaining significant experimental support from a rapidly accumulating body of work, which now includes many diverse cases spanning bacterial, fungal, plant, and animal cells. The most well-known examples are ribonucleoprotein (RNP) bodies[7] comprised of protein and

Received: January 18, 2019
Revised: March 8, 2019
Published: March 11, 2019

Downloaded via NANYANG TECHNOLOGICAL UNIV on May 2, 2019 at 01:54:17 (UTC).
See https://pubs.acs.org/sharingguidelines for options on how to legitimately share published articles.

ACS Publications © 2019 American Chemical Society

DOI: 10.1021/acs.biomac.9b00081
Biomacromolecules 2019, 20, 1709−1718

RNA molecules. Among others, these include Cajal bodies[8] and nucleoli[9] in the nucleus, which mediate ribonucleoprotein assembly, stress granules[10,11] and processing bodies[12] in the cytoplasm, of which the latter regulate RNA stability and protein translation in response to stress stimuli.[13,14] Other examples of intracellular liquid assemblies, which are composed only of protein molecules include clusters of signaling molecules, which "wet" the membrane surface such as during activation of T-cell receptors[15] and of actin nucleation factor.[16] Furthermore, mounting evidence now suggests that the errors in biological regulation of these condensates is often associated with the formation of extended gel- or solid-like protein aggregates,[17] which characterize many age-related pathologies, including cancer[18] and neurodegenerative diseases[19,20].

In all of these cases, although the number of different molecules present in single droplets is often large, only a handful are thought to be responsible for driving the condensate formation.[5,6,21] Recent studies focusing on the mechanisms of intracellular phase transitions invoke multivalency as the primary driving force: multiple low-affinity, transient interactions between interacting proteins such as what occurs in repetitive sequences of intrinsically disordered domains of low-sequence complexity, or prion-like domains.[22,23] Beyond a first threshold concentration, these multivalently interacting proteins undergo a molecular-level "sol−gel" transition, which drives liquid−liquid phase separation into protein-rich and protein-poor phases, at the macroscopic level. In close analogy with the thermodynamic phase separation of polymers, this process offset the loss of mixing entropy through chain-configurational entropy.[6,21] Moreover, these multivalent proteins, in many cases, upon exposure to non-native environments or crossing a second threshold in concentration above which the initial fluid droplets transform into irreversible gel- or solid-like condensates (e.g., amyloids) linking physiological droplets with pathological solids.

The realization that cytoplasmic condensates may act as efficient, functional supramolecular devices for establishing spatiotemporal control of cellular reactions raises an intriguing question: as with other cellular processes, are these droplet-producing phase separation and phase transition mechanisms vulnerable to viral hijacking?[24] As obligate intracellular pathogens, viruses derive their success by replicating within host cells. They achieve this, most frequently, by transiently assembling host-cytoplasmic compartments or virus replication organelles (VROs)[25] that sequester components from the virus (RNA and proteins) and the host (proteins, membranes and lipids). This assembly draws protection from host proteases and nucleases, suppressing competing host defense mechanisms, and enables viral replication.[26] A striking example is the so-called "membranous web" (MW) in the cytoplasm of cells infected by positive strand RNA viruses, such as Hepatitis C virus.[27] Acting as VROs,[28] these spatiotemporal clusters form by the remodeling of the endoplasmic reticulum (ER). They are composed of clusters of ER-derived vesicles, 80 to 180 nm in diameter and a number of viral proteins, replicating RNA, and a variety of host factors,[29] all packaged in a fluid amorphous matrix. Among viral proteins, a nonstructural protein, NS4B (27 kDa, 261 amino acids),[30] which is a highly hydrophobic integral membrane protein, is identified as the initiator of the MW formation by deforming the ER membrane.[30,31] Although the precise mechanisms by which NS4B induces local curvatures and topological divisions at the ER membrane surface needed to form precursor vesicles of the MWs are not known, a highly conserved, structurally resolved, and largely cytosolic N-terminal amphipathic α-helix domain (AH2), which extends from amino acids 42 to 66, is thought to play a critical role.[31,32] This α-helical domain may alter the ER membranes either by inserting the hydrophobic face at the headgroup-tail interface of the phospholipids[33] or by adopting a transmembrane conformation upon oligomerization.[34] Viewed from the lens of the fluid-condensate hypothesis, the MWs share functional characteristics with the cytoplamic droplets, but, the mechanisms of their biogenesis, their material properties, and modes of their activities are largely unknown. From a structural viewpoint, for instance, little is known about (1) the physical mechanisms driving the formation of MWs; (2) the material characteristics of the MW, including details of their phase state, microstructure, permeability, and mechanical properties; and (3) minimal requirements for the MW formation, including whether NS4B recruits other host proteins to form the membranous web or induces web formation by itself.

EXPERIMENTAL SECTION

Materials. Deuterium oxide (D_2O, 99.9%), DMSO-d_6 (99.9%), calcein, sodium chloride (NaCl, >99.5%), urea, tris(hydroxymethyl)-aminomethane (tris), sodium dodecyl sulfate (SDS) were purchased from Sigma-Aldrich. Phosphate-buffered saline (PBS) was from Vivantis Technologies (Selangor, Malaysia). 1,2-Dioleoyl-*sn*-glycero-3-phosphocholine (DOPC), 1-palmitoyl-2-oleoyl-*sn*-glycero-3-phosphocholine (POPC), egg sphingomyelin (SM), cholesterol, and lissamine rhodamine B 1,2-dipalmitoeyl-*sn*-glycero-3-phosphoethanolamine (Rhod-DPPE) were purchased form Avanti Polar Lipid (Alabaster, Alabama, USA). 4BAH2 (H-WRTLEAFWAKHMWNFIS-GIQYLA-NH2) were acquired from Anaspec Inc. (Fremont, CA). All chemicals were used without further purification. 96-well plates were obtained from Ibidi GmbH (Planegg/Martinsried, Germany).

Preparation of Large Unilamellar Vesicles (LUVs). Desired amounts of lipids in chloroform (DOPC, POPC or POPC/SM/Cholesterol, 1:1:1 molar ratio) were added to a glass tube. The chloroform was evaporated under nitrogen gas and subsequently dried under vacuum overnight. The dried lipid film was then rehydrated in Tris-buffered saline (150 mM NaCl, 10 mM Tris, pH 7.5) by brief vortexing and stirred for 2 h at 1−2.5 mg mL^{-1}. For LUVs prepared at pH 4 and pH 10, rehydration was performed in 5 mM Glycine buffer and sodium acetate buffer, respectively. The multilamellar vesicle suspensions were subsequently passed through an Avanti Mini-Extruder (Avanti Polar Lipids, Alabaster, AL) 21 times at room temperature for DOPC or POPC and at 50 °C for POPC/SM/Cholesterol LUVs. The extruder was assembled with 50, 100, 200, or 1000 nm polycarbonate membranes and two 1 mL gastight syringes from Hamilton (Reno, NV). The vesicles were then used immediately or stored in small centrifuge tubes at 4 °C. Vesicles size distributions were verified by dynamic light scattering using Particle Size Analyzers by Brookhaven Instruments Corp. (Holtsville, NY, USA). For fluorescence microscopy experiments, 0.1 mol % Rhodamine-DPPE was added to the initial chloroform-dissolved lipids in glass tubes.

Preparation of 4BAH2 Peptide Stock Solutions. 4BAH2 was dissolved to a stock concentration of 340−690 μM (H_2O + 5% v/v DMSO) and was divided into aliquots and stored in the freezer at −20 °C.

Time-Lapse Photography. Vesicle solutions were diluted to 0.4 mg/mL in a cuvette and 4BAH2 was added by using a manual pipet slowly (5−10 s) to a final concentration of 2.5−10 μM. Time-lapse images were captured using a iPhone 6 or iPhone 7 (Apple Inc., Cupertino, California) at 30 or 60 frames per second. Contrast-enhanced images were prepared using Fiji.[35]

Preparation of Giant Unilamellar Vesicles (GUVs). A 1 mg mL^{-1} lipid stock of POPC, doped with a 1 mol % of Rho-DPPE was prepared. 20 μL of the lipid mixture (20 μg) was deposited on a clean ITO-coated glass slide and dried under vacuum for 1 h. The dried lipid

DOI: 10.1021/acs.biomac.9b00081
Biomacromolecules 2019, 20, 1709−1718

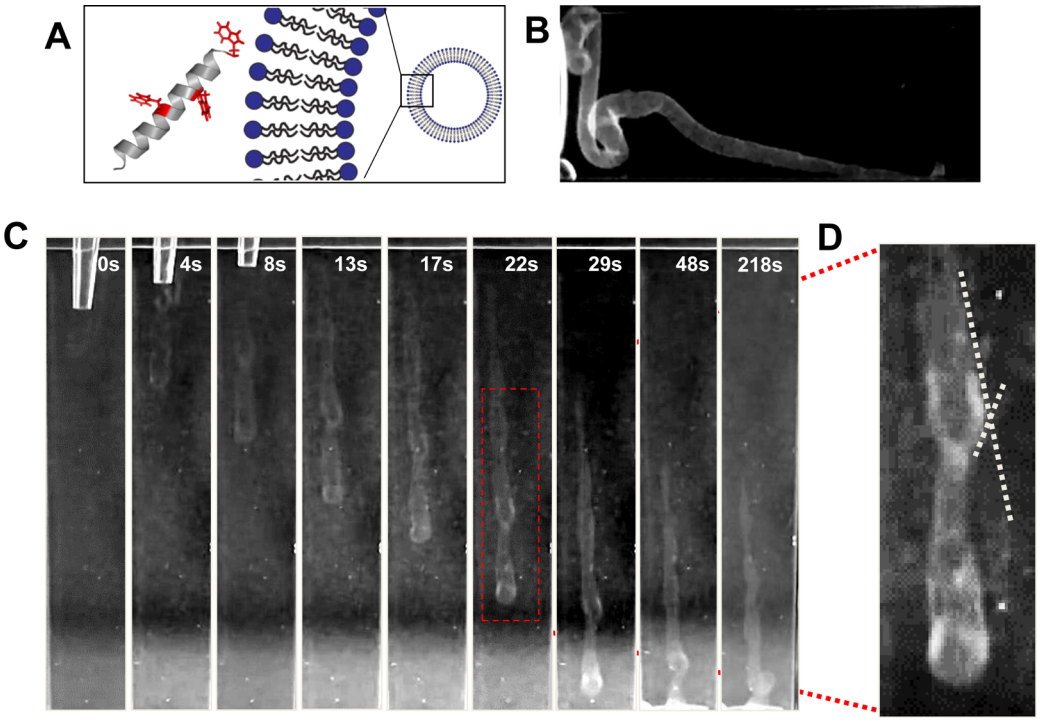

Figure 1. Macroscopic sol−gel transition of 4BAH2 and large unilamellar vesicles (LUVs). (A) The minimal, two components required for gel formation. (B) A typical contrast-enhanced photograph of the gel. (C) Time-lapse photography of the gel formation when 5 ul of 4BAH2 (575 μM) peptide was pipetted into a LUV suspension (0.4 mg/mL). (D) Enlargement of a selected region (from t = 22 s in C) highlights the angled structure (dotted lines) of the gel.

cake was flooded with 225 μL of 200 mM sucrose within an area delimited by an O-ring, and covered with a second ITO-coated glass slide. Electroformation[36] was carried out at 25 °C with application of an AC current at 5 Hz and 3 V for 120 min. The GUVs were suspended in the isotonic glucose solution of identical osmolarity for microcopy imaging on an inverted Eclipse TE 2000 microscope (Nikon) fitted with an Andor iXon+ EMCCD camera (Andor Technology, Belfast, Northern Ireland).

Wide-Field fluorescence Microscopy. DOPC LUVs doped with 0.1 mol % of Rhod-DPPE were prepared as described above and diluted to approximately 0.4 mg/mL in Tris-buffered in a 96-well plate. 4BAH2 was added to a final concentration 1−2.5 μM. Images were captured on an inverted Eclipse TE 2000 microscope (Nikon) fitted with an Andor iXon+ EMCCD camera (Andor Technology, Belfast, Northern Ireland). Samples were visualized using a 60× oil immersion objective (NA 1.49) or a 20× objective and TRITC (Rhod-DPPE) and FITC (calcein) filter sets with a mercury lamp (Intensilight C-HGFIE; Nikon Corporation).

Fluorescence Recovery after Photobleaching (FRAP). LUVs solution was diluted to 0.4 mg/mL in a 96-well plate and 4BAH2 was added by using a manual pipet slowly (5−10 s) to a final concentration of 2.5 μM. Images were captured on an inverted Eclipse TE 2000 microscope (Nikon) fitted with an Andor iXon+ EMCCD camera (Andor Technology, Belfast, Northern Ireland). FRAP experiments were performed with a 50 mW 561 laser line. The gel was viewed with a 60× oil immersion objective (NA 1.49) and Rhod-DPPE probe was bleached in a circular region (diameter = 10 μm) at maximum laser power for 7 s. Four prebleached frames with an interval of 2 s were recorded and the recovery of fluorescence was measured up to 2400 s with an interval of 30 s.

The fluorescence recovery curve of each gel area studied was fitted to a double term equation ($I_{fit2} = I_0 - ae^{-\beta t} - \gamma e^{-\delta t}$) and the half-time for recovery, $t_{1/2}$ was computed using EasyFRAP-web.[37] The diffusion coefficient, D, was calculated using $D = ({r_e}^2 + {r_n}^2)/8t_{1/2}$,[38] where r_n is the radius of the user-defined bleached spot and r_e is the effective radius calculated from the postbleach profile, estimated in Fiji.

Dye Permeation Assay. Calcein was dissolved in small amount (0.5 mL) of 1 M NaOH and PBS was added to reach a final concentration of 50 mM and pH was adjusted to pH 7.5. LUVs solution was diluted to 0.4 mg/mL in a 96-well plate and 4BAH2 was added by using a manual pipet slowly (5−10 s) to a final concentration of 2.5 μM to form a gel. The gel was let to settle for about 10 min. Calcein was then added to a final concentration of 50 μM and the preformed gel was incubated for 10 min. The excess calcein in the LUVs solution was serially diluted and the fluorescence images of the calcein-loaded gel were captured on an inverted Eclipse TE 2000 microscope (Nikon) fitted with an Andor iXon+ EMCCD camera (Andor Technology, Belfast, Northern Ireland). Samples were visualized using a 60× oil immersion objective (NA 1.49) or a 20× objective and FITC (calcein) filter sets with a mercury lamp (Intensilight C-HGFIE; Nikon Corporation).

Infrared Spectroscopy. Infrared measurements were performed on a Vertex 70 (Bruker, Ettlingen, Germany), equipped with a MIRacle (PIKE Technologies, Madision, Wisconsin, USA) attenuated total reflection unit, which contained a single reflection diamond (angle of incidence = 45°). During the measurements, the spectrometer was purged with N_2 gas to remove CO_2 and water vapor. Spectra were recorded with a spectral resolution of 4 cm^{-1} in double-sided acquisition mode with a photovoltaic liquid nitrogen cooled mercury cadmium telluride detector. Static measurements were taken with 1500 scans. For kinetic measurements, spectra were taken at a 1 min interval. Spectra were calculated using a Blackman-Harris 3-term apodization function and zero filling factor of 2. 4BAH2 was dissolved in D_2O, which contains 5% DMSO-d_6 by volume and adsorbed on the surface of the surface of the ATR-element over 45 min. 50 nm DOPC LUVs solution (2.5 mg/mL) were added and incubated for 45 min. In another experimental setup, the sequence of addition of peptide and LUVs solution was reversed. Data acquisition and analysis were done with OPUS 6.5 and OriginPro 2015.

Tryptophan Fluorescence Spectroscopy. Fluorescence emission scans (Ex = 295 nm, Em = 330−355 nm) were collected for 4BAH2 alone and a mixture of 4BAH2 and LUV, prepared as described above, at pH 4, pH 7.5 and pH 10. 4 M urea and SDS were subsequently

DOI: 10.1021/acs.biomac.9b00081
Biomacromolecules 2019, 20, 1709−1718

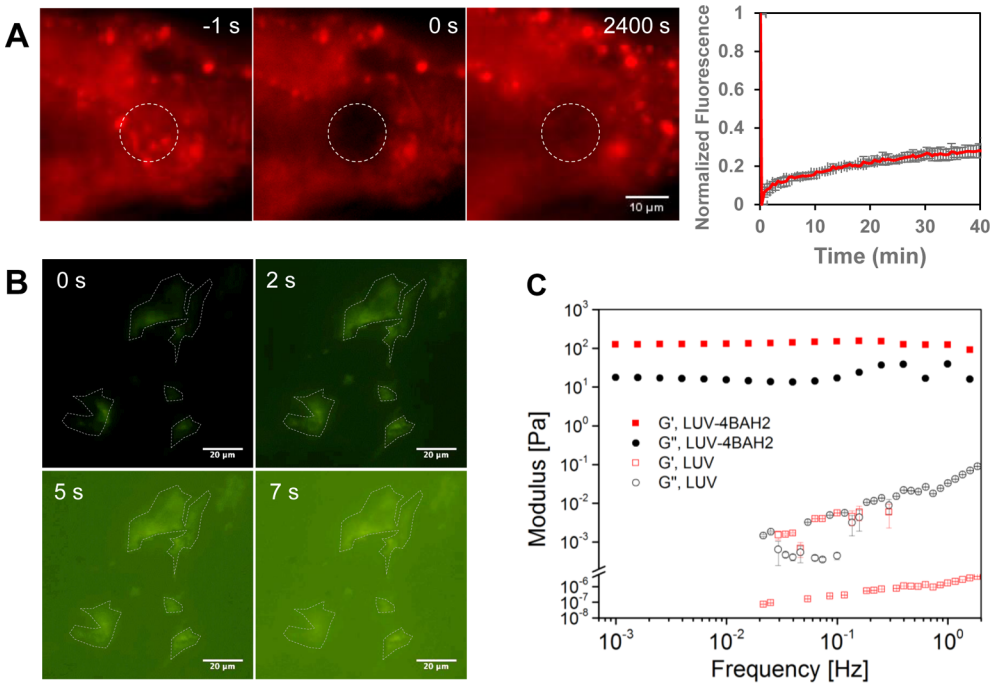

Figure 2. Characterization of lateral diffusion of phospholipid vesicle, molecular permeation and viscoelastic properties of the gel. (A) *Left panel.* Selected fluorescence image sequences of a 0.1% Rhodamine-DPPE doped gel. Fluorescence was monitored before and directly after photobleaching, up to 2400 s. *Right panel.* Normalized fluorescence recovery curves for FRAP experiments showing average of independent measurements of two different spots on the gel. (B) Molecular permeation assay of loading and unloading of calcein. Gel is formed in calcein-free solution and exposed to calcein (50 μM), followed by dilution of the free calcein in the gel exterior (t = 0 s). (C) Frequency sweep measurements of storage (G'; red) and loss (G''; black) moduli of the gel (closed symbols) and LUV suspension (open symbols).

added and the emission scans were collected. Intensity values at 340 nm from the emission scans were plotted as a function of time. The experiments were repeated 3−5 times.

Cryogenic Electron Microscopy. Electron microscope grids, coated with a holey carbon film (R2/2 Quantifoil without 2 nm carbon), were glow discharged. A gel was prepared by pipetting 5 μL peptide stock (575 μM) into 50 μL LUVs solution (2 mg/mL). 4 μL of gel-containing solution was deposited onto a grid at 99% humidity, blotted with filter paper (2 s blotting time, 0 blot force), and plunged into liquid ethane (Vitrobot, FEI Company). Cryo-grids were imaged using a FEG 200 keV transmission electron microscope (Arctica, FEI Company) equipped with a direct electron detector (Falcon II, Fei Company). Images were recorded at a nominal 53 000× magnification with an integration time (exposure time) of 1 s. Line scans to plot density distribution across high- and low-density features were carried out in Fiji.[35]

RESULTS AND DISCUSSION

In the work reported here, we demonstrate a minimal *in vitro* reconstitution model of the membranous web. We find that the N-terminal amphipathic domain of NS4B (4BAH2 peptide) and large unilamellar phospholipid vesicles (~100−200 nm in diameter, LUVs) represent the minimal number of components needed to produce MW-like assemblies (Figure 1): A simple incubation of the two constituents, amphipathic peptide and the lipid mesophase, triggers a striking isothermal, sol−gel transition producing a gel-like viscoelastic condensate, which stably coexists with the surrounding medium (Figure 1), reminiscent of the virus-induced membranous web. More generally, our results suggest that the biogenesis of condensed cytoplasmic phases is not confined to multivalent, intermolecular RNA-protein or protein−protein interactions alone, but rather supramolecular assemblies (i.e., vesicles) can spatially template effective multivalency *de novo* between otherwise weakly interacting proteins.

We began by pipetting aliquots (5 μL) of the buffered solutions of peptide 4BAH2, which presents the AH2 domain sequence of NS4B (50−500 μM), into a 1 mL suspension of LUVs (0.4 mg/mL, 100−200 nm in diameter) composed of a simple phospholipid, namely, 1-palmitoyl-2-oleoyl-*sn*-glycero-3-phosphocholine (POPC) in the same buffer (see Experimental Section). When the concentrations of peptide solutions were low (<50 μM), the solutions remained clear. Above this threshold, however, a new phase demixed instantaneously (Figure 1). Here, during a slow and continuous pipetting of the peptide solution (>50 μM aliquots), a translucent phase emerged at the point of contact, which grew as more peptide was added producing a remarkable macroscopic columnar phase floating in the surrounding aqueous environment (Video S1). When aliquots were added in multiple steps, each step produced a separate translucent phase suggesting a kinetically controlled gelation. Quite frequently, the emergent columnar phase displayed a striking beads-on-a-string (BOAS) morphology[39] elongated along its long axis, reminiscent of capillary thinning of threads of viscoelastic fluids subject to linear stretches. This simple and casual observation provides an early hint for the incipient sol−gel transition suggesting the formation of a viscoelastic phase prompted by the interaction of the peptide with the vesicle. Unlike the conventional evolution of the BOAS morphologies, the translucent, columnar phase, however, did not breakup, but rather evolved into a sheet-like morphology with nonspherical boundaries over the course of several seconds. The angled morphology is further consistent with the incipient sol−gel transition (Figure 1d).

DOI: 10.1021/acs.biomac.9b00081
Biomacromolecules 2019, 20, 1709−1718

If left undisturbed, the translucent gel-like phase remained stable for days, even months. The solutions could be shaken without disturbing the gross morphology of the translucent phase, but not stirred. Vigorous stirring unraveled the macroscopic morphology yielded finer aggregates, which remained suspended in the aqueous solution. Examination of these "aggregates" under optical microscope revealed microscopic particles of arbitrary, irregular shapes, which did not spontaneously merge or coalesce, consistent with their gel-like properties (Figure S1). Moreover, when we incubated the peptide with fluorescently doped LUVs containing a small proportion of (~0.1 mol %) Rhodamine-DPPE, the gel phase acquired the lipid fluorescence confirming the accumulation of the lipid component within the gel. The ratio of fluorescence intensity in the gel-like phase and the surrounding bulk revealed 5−15-fold enrichment of vesicles in the gel-like condensates. Moreover, we employed a fluorescence recovery after photobleaching (FRAP) experiment to measure the diffusivity of intact vesicles within the condensates, in analogy to measuring lateral diffusivity of phospholipid within a bilayer. This microscopy-based test revealed the long-range diffusivity of fluorescently doped vesicles within the condensed phase to be $D = 6\ (\pm 2) \times 10^{-10}$ cm^2 s^{-1} with a significant immobile fraction of >50% (Figure 2a). Contrasting with the diffusion of free vesicles ($D_{free} \sim 1-10 \times 10^{-8}$ cm^2 s^{-1}) in water,[40] this represents a 2 orders of magnitude slower mobility of the constituent vesicles entrapped in the condensed phase. Such drastic reduction in mobilities of vesicles, under otherwise comparable conditions, can be readily attributed to changes in solution viscosities. For example, a previous study has shown that the presence of 5 mg/mL mucin, which elevates the solution viscosity by 50% ($\frac{\eta}{\eta_o} \geq 1.5$, where η is the solution viscosity and η_o, the solvent viscosity), lowers vesicular mobilities by a full order of magnitude in comparison with pure water.[41,42] Based on the above, it seems reasonable that the condensed gel-like phase presents a highly viscous environment for the encapsulated vesicles.

This concentration-dependent and peptide-induced sol−gel transition of a vesicular suspension appeared to weaken with less intense remodeling at acidic pH (below the pK_a of 4BAH2), suggesting the importance of ionic interactions for the phase transition (corresponding data is presented later in Figure 4a). This is further confirmed by the observations that the exposure to ionic detergent (SDS) dissolved the gel, but a nonionic detergent (triton x-100) failed to induce any measurable change.[43] Moreover, the phase transition producing the gel-like phase was not affected by the chemical composition of the constituent vesicles, but depended strongly on the curvature of the vesicles. Replacing the single phospholipid, i.e., POPC, with a mixture consisting of DOPC, sphingomyelin, and cholesterol at equimolar ratio, which mimics the essential lipid composition of the membranous web and the viral envelope,[44,45] yielded qualitatively similar results (Figure S2a). But when LUVs (~100−1000 nm in diameter) (Figure S2b) were replaced with giant vesicles (>10 μm in diameter), the gel formation was noticeably suppressed. This then suggests, but does not conclusively establish, the plausible role of nanometer scale curvatures of LUVs in promoting the sol−gel transition (Figure S3). Additional experiments using vesicles of systematically varied curvatures under comparable solution conditions are needed to accurately determine the importance of vesicular curvatures in facilitating the observed sol−gel transition.

The condensate hypothesis for the living cell stipulates an important requirement for their functionality: an ability to not only sequester specific biochemicals in their interior but also exchange molecules (and signals) with their surrounding cytoplasmic environment. To determine whether the minimal membranous web-like phase demonstrated here is also capable of exchanging molecules with the environment, we carried out molecular permeation assays. We incubated a preformed gel in the calcein-laden solution for ~10 min followed by the exchange of solution using calcein-free buffer. A simple examination of the calcein-exposed gel under a fluorescence microscope yielded a clear evidence of the molecular uptake: the gel was rendered fluorescent. Over time, the fluorescent gel gradually released the trapped calcein as seen in the gradual increase in the fluorescence intensity of the surrounding solution (Figure 2b). This simple test, further confirmed by FRAP measurements, establishes that the lipido-peptide, gel-like condensate is indeed permeable, capable of exchanging small molecules with its aqueous environment.

To quantify the viscoelastic characteristics of the condensates, we carried rheological measurement. After a careful removal of the bulk vesicle suspension, we subjected the residual condensate gel to sweeps of shear oscillations in amplitude to identify the linear viscoelastic (LVE) regime for the gel response. Within the LVE regime, we chose 0.3% strain for subsequent frequency sweeps measurements to deduce the complex viscoelastic modulus of the condensed phase. The results (Figure 2c) reveal that the elastic (or storage) modulus dominated the response over the viscous (or loss) modulus at all frequencies, $G'(\omega) > G''(\omega)$, a clear confirmation that the condensate exhibits gel-like viscoelastic characteristics. The absolute values of the two moduli fell in the ranges of 20−100 Pa for G' and 2−20 Pa for G'' across multiple independent measurements suggesting the formation of a weak physical gel.[46] As expected, parallel measurements of vesicle suspension alone (without peptide) produced an essentially liquid-like response comparable to that of aqueous suspensions or water.

What is inside the condensates? To identify the molecular constituents of the newly formed gel phase, we used attenuated total reflection-Fourier transform infrared spectroscopy (ATR-FTIR) measurements. The spectra of the air-dried (or lyophilized) gels deposited directly onto the infrared reflection element displayed peaks due to two sets of characteristic group frequencies: (1) a low-frequency peak at approximately 1645 cm^{-1}, corresponding to the Amide I band, which originates from the C═O stretching vibration of the amide group coupled with the in-phase bending of the N—H bond and stretching of the C—N bond[47] and (2) a high frequency absorption envelope consisting of peaks at ~2850 and ~2918 cm^{-1} due to methylene C—H symmetric (d^+) and antisymmetric (d^-) stretching vibrations,[48] respectively (Figure 3a). The former, amide I absorption peak, confirmed the incorporation of the peptide and the latter, the vesicles in the incipient gel.

To better characterize the gel formation process, we monitored the spectral response in real-time by adding the peptide onto lipid vesicles presettled onto an ATR crystal (Figure S4a). Immediately after the addition of the peptide, the peak due to the peptide-associated Amide I band (~1650 cm^{-1}) appeared, and grew monotonically over the course of next 20 min. Concomitantly, the intensities due to the methylene vibrational modes (2925 and 2854 cm^{-1}) also increased suggesting the recruitment of additional vesicles at the vesicle-laden crystal interface in the presence of the peptide. Repeating

DOI: 10.1021/acs.biomac.9b00081
Biomacromolecules 2019, 20, 1709−1718

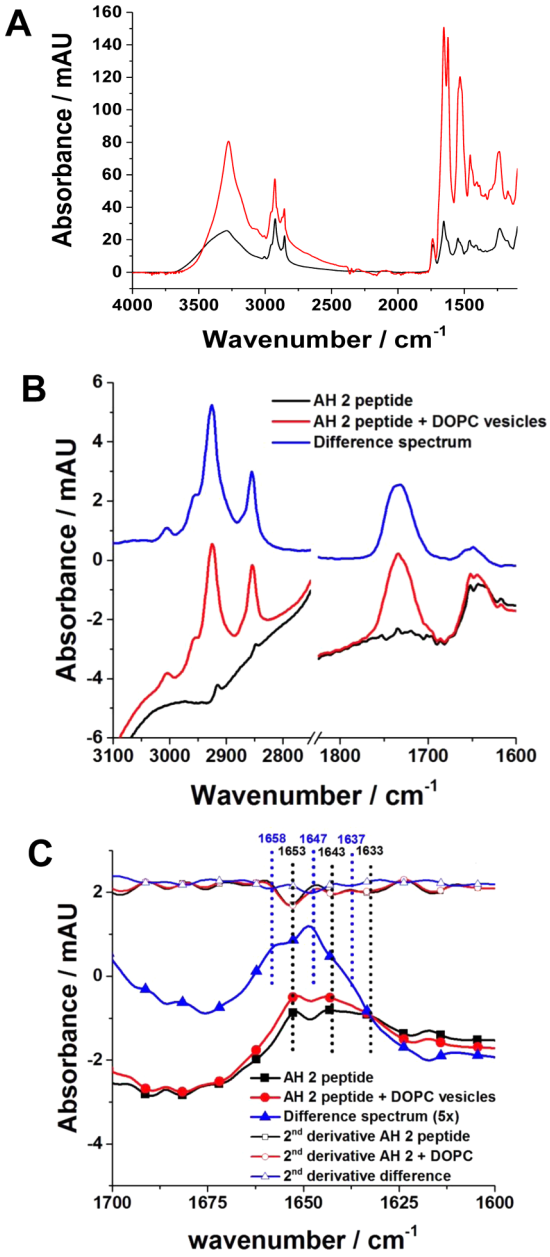

Figure 3. Compositional characterization of the gel by ATR-FTIR spectroscopy. (A) Absorbance spectra of the air-dried (red) or lyophilized (black) gels deposited directly onto the infrared reflection element. (B) Absorbance spectra after 4BAH2 incubation (black) and after subsequent LUVs addition (red) at liquid state. The difference spectrum (blue = red-black) is overlaid. (C) 2nd derivatives (lines with open symbols) of the absorbance spectra (lines with closed symbols) after 4BAH2 incubation (black) and after LUV addition (red) from 1600 to 1700 cm^{-1}. The difference spectrum (blue) and 2nd derivative spectra show an upshift of the Amide I bands.

the experiment by switching the order in which the two gel forming components are presented to the ATR surface, adding vesicles to the crystal surface presaturated with the peptide, confirmed the foregoing inference (Figure S4b). Here, the addition of vesicles instantaneously increased the intensities due to methylene C—H stretching vibrations while increasing the intensity of the Amide I band further (Figure 3b). Together, these observations document the cooperative nature of interactions between the precursor vesicles and the peptide driving the growth of the gel-like condensate.

The position of the Amide I band is a sensitive indicator of the peptide's secondary structure. The dominant peak at 1658 cm^{-1} can be readily assigned to the predominantly α-helical structure.[49] Because of the differences in the patterns of H-bonding and local geometric orientations of amide bonds in secondary structural folding including α-helices, β-sheets, β-turn and random coil, precise positions of the components of the Amide I envelope sheds further light on the peptide structure in the gel. In the present case, a comparison of the positions of the Amide I components (resolved using second derivatives of the spectral envelopes) between the free peptide and that conjugated with lipid vesicles in the gel reveal noticeable shifts from the positions of 1653, 1643, and 1633 cm^{-1} (free peptide) to 1658, 1647, and 1637 cm^{-1} (gel), respectively (Figure 3c). These shifts are consistent with the changes the H-bonding bridges of the α-helical peptide[50−52] and those between the amphipathic peptide and the membrane as it integrates into the viscoelastic gel architecture.

To further assess the nature of interactions between the peptide and the vesicles driving the gel formation, we monitored the changes in the intrinsic tryptophan (Trp) fluorescence, a diagnostic marker of the polarity of the local environment within which the fluorophore resides.[53] We found that the addition of 4BAH2 to a vesicle suspension led to a rapid increase in the Trp fluorescence intensity (Figure 4b). These observations indicate the shift in the microenvironment for the Trp residues on 4BAH2 from the polar environment of the aqueous phase to the less polar environment, likely because of their plausible localization at the membrane interfaces (see below).

Next, we sought to address how the coexisting vesicular and peptide components are spatially organized in the gel using cryo-electron microscopy (cryo-EM) measurements. We prepared the samples by flash-freezing the gels isolated from the precursor aqueous solution using liquid ethane and imaged in thin vitrified amorphous ice layer, unfixed and unstained. The images display a strikingly ordered organization characterized by a honeycomb-like lattice extending across the entire imaged area suggesting templated hierarchy in the organization of the vesicular and peptide components (Figure 5 and Figure S5).

To deduce details about the spatial organization in the gel, we next examined electron scattering profiles. Plotting the scattered intensities across line scans over several honeycomb cells reveal several noteworthy features of the gel organization. First, an average linear dimension of individual cells in the honeycomb lattice estimated at 91 ± 19 nm (n = 35). Moreover, a dark band of uniform width delimited the honeycomb cells, which averaged at 4.16 ± 0.67 nm (n = 30). The former value is consistent with the size of a single vesicle and the latter, the thickness of a single bilayer bounding the vesicle, together suggesting an ordered lattice-like assembly of deformed vesicles. Second, we found that the spacing between neighboring cells is 3.79 ± 0.83 nm (n = 80). Assuming the major scattering portions in the gel are the hydrophilic headgroups of the lipids, the uniform density distribution of the dark bands suggests that the membrane of the deformed vesicles are structurally preserved across the vesicle perimeter. What then determines the spacing between the vesicles? Based on a previously solved solution NMR structure of a NS4B consensus sequence,[31] 4BAH2 is approximately 3.3 nm in length. Considering the small size of 4BAH2 (>10 times smaller than the theoretical lower size limit of cryo-EM for unstained biological sample −2.8 kDa against 38

DOI: 10.1021/acs.biomac.9b00081
Biomacromolecules 2019, 20, 1709−1718

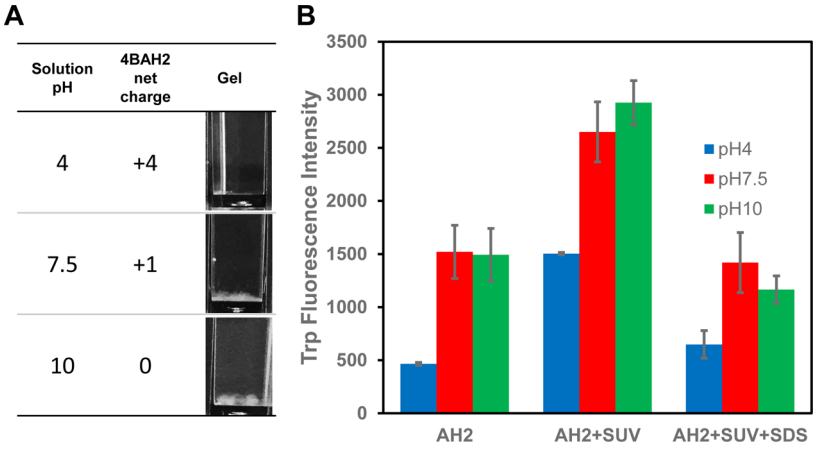

Figure 4. Gel formation and intrinsic tryptophan fluorescence measurement as a function of pH. (A) Photographs of gels formed at pH 4, 7.5, and 10. (B) Intrinsic tryptophan fluorescence measurement of free 4BAH2 in solution, 4BAH2 in gel and when the gel is treated with 4 M urea and further dissolved by SDS, as a function of pH. Error bars are standard deviations of 3−5 independent measurements.

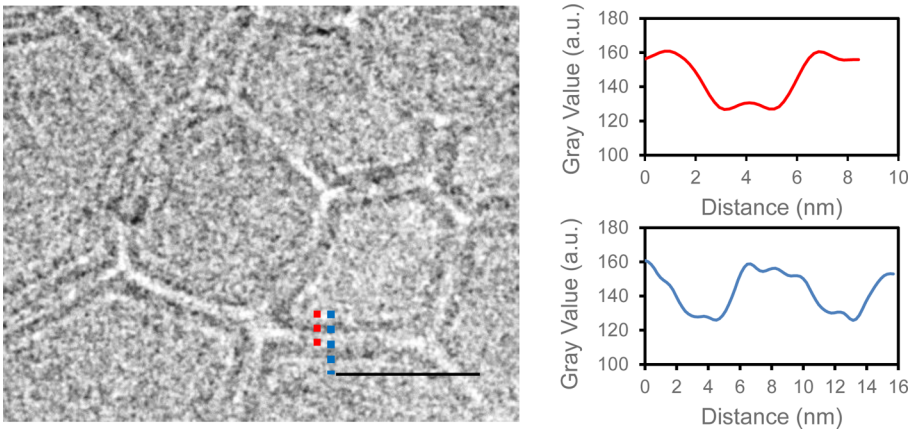

Figure 5. Cryo-EM images of peptide−vesicle gel. *Left*. Micrograph of closely packed polygonal-shaped vesicles with tight intervesicle spacing. *Right*. Red and blue dotted lines indicate line-scan regions of the line profiles.

kDa) and its propensity of self-association, we ascribe the low-density region to a rim of peptides and the high-density region to the phospholipid bilayers of the constituent vesicles. These results lend direct support to the cooperative assembly of 4BAH2 and nanometer-sized spherical lipid vesicles into a membranous gel, characterized by closely packed polygonal-shaped vesicles with tight intervesicle spacing.

CONCLUSION

The cumulated weight of the results above suggests a unifying picture for the 4BAH2-mediated gel formation in vesicular suspensions, such as proposed below (Figure 6). As an amphipathic peptide characterized by segregated distribution of hydrophobic and polar residues between the opposite faces of the α-helix, 4BAH2 is known to undergo self-oligomerization in aqueous solution.[34] Here, hydrophobic forces drive multiple copies of the peptide, four by one estimate,[54] to undergo self-assembly producing an oligo-helical bundle. In the presence of LUVs, however, this tendency for hydrophobically driven self-oligomerization is necessarily altered because of interaction between the polar face of the amphipathic 4BAH2 peptides and the dipolar headgroups of the phospholipids comprising the membrane.[43] This peptide−vesicle association replaces the monomeric amphipathic peptide with a novel peptido-vesicular building block, which exposes the hydrophobic face of the bound peptides to the aqueous solution. Viewed from the vantage of the vesicles, the solvent-exposed hydrophobic faces of the bound peptides render the LUVs "sticky." The ensuing peptide−peptide self-association must now occur in tandem with the vesicular "cargo". Because several copies of the "sticky" peptides are expected to be displayed on single LUVs, which renders the peptide−vesicular building blocks multivalent, the ensuing peptide oligomerization links the vesicular "cargo" in a three-dimensional network, which separate away from the bulk aqueous solution forming extended gel-like condensates. Curiously, this mode of inducing colloidal sol−gel transition is reminiscent of the notion of "colloidal molecules," where synthetic colloidal particles, not unlike vesicles in the present case, decorated with "sticky patches," consisting of dimerizing oligonucleotides, functionally comparable to peptides in our case, were shown to produce programmable multivalent interactions between particles through patch−patch interactions.[55]

This mode of condensate formation, which we call programmable multivalency, is clearly unique, different from all other mechanisms of droplet (and gel) formation in the cytoplasmic space. Recent studies have identified multivalent self-association and cross-association between extant polymeric biomolecules. Our proposed model suggests that the living cell can create multivalency *de novo* enabling otherwise discretely interacting

DOI: 10.1021/acs.biomac.9b00081
Biomacromolecules 2019, 20, 1709−1718

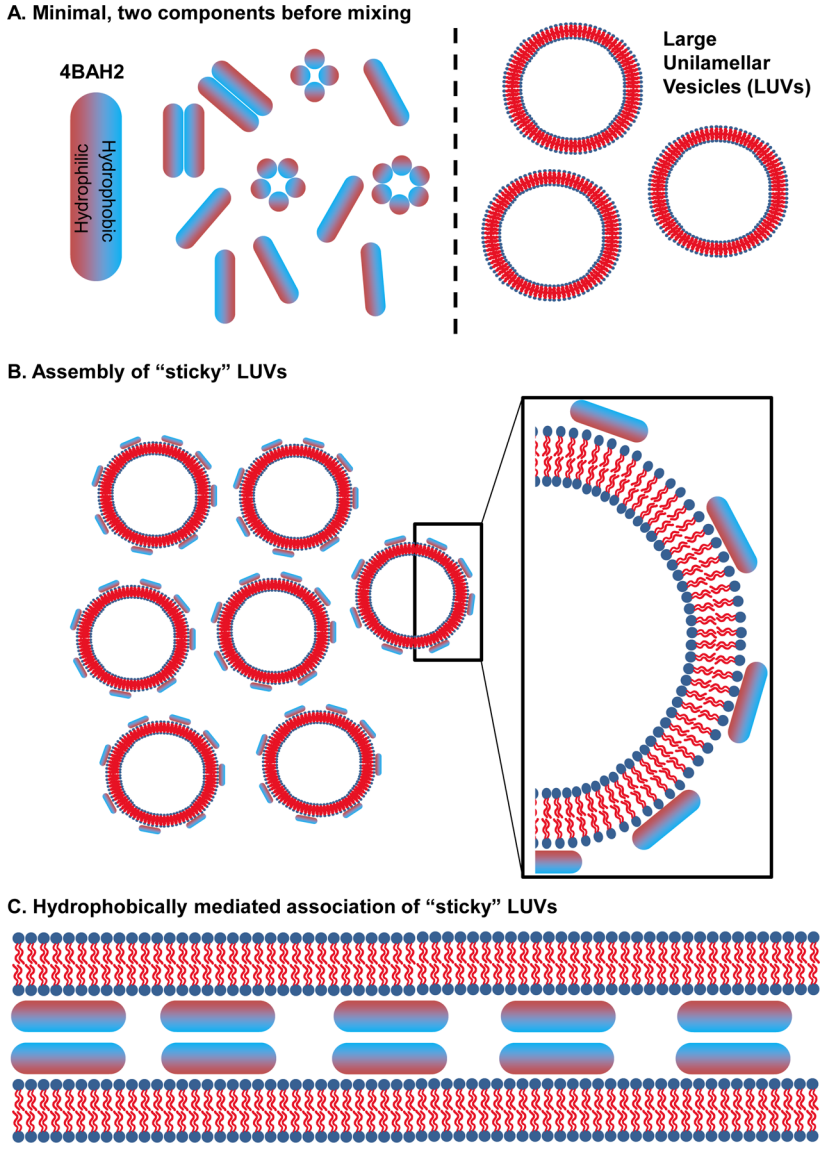

Figure 6. Proposed mechanism for peptide−vesicle sol−gel transition. (A) The two, minimal components required for vesicle−peptide sol−gel transition. *Left*. 4BAH2, depicted as an amphiphilic cylinder consisting of a hydrophobic (blue) and a hydrophilic (orange) face. Driven by hydrophobic association, 4BAH2 may exist as oligo-helical bundles in solution. *Right*. Cross sections of LUVs with the polar headgroups (blue) and the nonpolar phospholipid tails (red). (B) In the presence of LUVs, the polar face of 4BAH2 binds to the dipolar headgroups of the phospholipids, decorating a single LUV with multiple copies of "sticky" peptides. (C) The peptide−peptide self-association occurs with the vesicular cargo. The binding of multiple copies of the "sticky" peptides renders the peptidovesicular building blocks multivalent and the ensuing peptide oligomerization links the vesicular "cargo" in a three-dimensional network, forming extended gel-like condensates.

moieties to achieve multivalency and drive condensate formation. The viruses, again, appear to have hijacked a generic cellular mechanism, this time a physical-chemical mechanism of phase separation, to their own benefit.

■ ASSOCIATED CONTENT

Supporting Information

The Supporting Information is available free of charge on the ACS Publications website at DOI: 10.1021/acs.biomac.9b00081.

Optical microscopy image of microscopic particles of arbitrary shapes; peptide−vesicle sol−gel transition as a function of vesicle size, lipid composition and incubation time; membrane effect on GUVs mixed with 4BAH2; real-time ATR-FTIR measurement of Figure 3; additional cryo-EM images of the peptide−vesicle gel (PDF)

Time-lapse video of the sol−gel transition (AVI)

■ AUTHOR INFORMATION

Corresponding Authors

*Bo Liedberg (bliedberg@ntu.edu.sg).

*Atul N. Parikh (anparikh@ucdavis.edu).

ORCID

Ali Miserez: 0000-0003-0864-8170

NamJoon Cho: 0000-0002-8692-8955

Atul N. Parikh: 0000-0002-5927-4968

Bo Liedberg: 0000-0003-2883-6953

Notes

The authors declare no competing financial interest.

DOI: 10.1021/acs.biomac.9b00081
Biomacromolecules 2019, 20, 1709−1718

■ ACKNOWLEDGMENTS

J.C.S.H., A.N.P. and B.L acknowledge support from the Provost Office and the School of Materials Science & Engineering, Nanyang Technological University. C.S. and E.R. are funded by the City of Vienna and the International Graduate School Bio-Nano-Tech. S.H.H and A.M acknowledge financial support from the Singapore National Research Foundation (NRF) through a NRF Fellowship awarded to A.M., and from a Singapore Ministry of Education (MOE) Academic Tier 2 grant (Grant MOE 2011- T2-2-044). N.J.C and M.C.K acknowledge support from the National Research Foundation (NRF-NRFF2011-01) and NRF POC and Nanyang Technological University.

■ ABBREVIATIONS

4BAH2, N-terminal amphipathic domain of NS4B; LUV, large unilamellar vesicles

■ REFERENCES

(1) Wilson, E. B. The Structure of Protoplasm. *Science* **1899**, *10*, 33−45.
(2) Hyman, A. A.; Simons, K. Beyond Oil and Water-Phase Transitions in Cells. *Science* **2012**, *337* (6098), 1047−1049.
(3) Shin, Y.; Brangwynne, C. P. Liquid Phase Condensation in Cell Physiology and Disease. *Science* **2017**, *357* (6357), 1253.
(4) Dolgin, E. Cell Biology's New Phase. *Nature* **2018**, *555* (7696), 300−302.
(5) Hyman, A. A.; Weber, C. A.; Juelicher, F. Liquid-Liquid Phase Separation in Biology. In *Annual Review of Cell and Developmental Biology*; Schekman, R., Lehmann, R., Eds.; Annual Reviews: Palo Alto, 2014; Vol. *30*, pp 39−58.
(6) Brangwynne, C. P.; Tompa, P.; Pappu, R. V. Polymer Physics of Intracellular Phase Transitions. *Nat. Phys.* **2015**, *11* (11), 899−904.
(7) Zhu, L.; Brangwynne, C. P. Nuclear Bodies: The Emerging Biophysics of Nucleoplasmic Phases. *Curr. Opin. Cell Biol.* **2015**, *34*, 23−30.
(8) Handwerger, K. E.; Cordero, J. A.; Gall, J. G. Cajal Bodies, Nucleoli, and Speckles in the Xenopus Oocyte Nucleus Have a Low-Density, Sponge-Like Structure. *Mol. Biol. Cell* **2005**, *16* (1), 202−211.
(9) Brangwynne, C. P.; Mitchison, T. J.; Hyman, A. A. Active Liquid-like Behavior of Nucleoli Determines Their Size and Shape in Xenopus Laevis Oocytes. *Proc. Natl. Acad. Sci. U. S. A.* **2011**, *108* (11), 4334−4339.
(10) Wheeler, J. R.; Matheny, T.; Jain, S.; Abrisch, R.; Parker, R. Distinct Stages in Stress Granule Assembly and Disassembly. *eLife* **2016**, *5*, DOI: 10.7554/eLife.18413.
(11) Wippich, F.; Bodenmiller, B.; Trajkovska, M. G.; Wanka, S.; Aebersold, R.; Pelkmans, L. Dual Specificity Kinase DYRK3 Couples Stress Granule Condensation/Dissolution to mTORC1 Signaling. *Cell* **2013**, *152* (4), 791−805.
(12) Brangwynne, C. P.; Eckmann, C. R.; Courson, D. S.; Rybarska, A.; Hoege, C.; Gharakhani, J.; Julicher, F.; Hyman, A. A. Germline P Granules Are Liquid Droplets That Localize by Controlled Dissolution/Condensation. *Science* **2009**, *324* (5935), 1729−1732.
(13) Bergeron-Sandoval, L. P.; Safaee, N.; Michnick, S. W. Mechanisms and Consequences of Macromolecular Phase Separation. *Cell* **2016**, *165* (5), 1067−1079.
(14) Wu, H.; Fuxreiter, M. The Structure and Dynamics of Higher-Order Assemblies: Amyloids, Signalosomes, and Granules. *Cell* **2016**, *165* (5), 1055−1066.
(15) Su, X. L.; Ditlev, J. A.; Hui, E. F.; Xing, W. M.; Banjade, S.; Okrut, J.; King, D. S.; Taunton, J.; Rosen, M. K.; Vale, R. D. Phase Separation of Signaling Molecules Promotes T Cell Receptor Signal Transduction. *Science* **2016**, *352* (6285), 595−599.
(16) Banjade, S.; Rosen, M. K. Phase Transitions of Multivalent Proteins Can Promote Clustering of Membrane Receptors. *eLife* **2014**, *3*, DOI: 10.7554/eLife.04123.
(17) Alberti, S.; Hyman, A. A. Are Aberrant Phase Transitions a Driver of Cellular Aging? *BioEssays* **2016**, *38* (10), 959−968.
(18) Boulay, G.; Sandoval, G. J.; Riggi, N.; Iyer, S.; Buisson, R.; Naigles, B.; Awad, M. E.; Rengarajan, S.; Volorio, A.; McBride, M. J.; Broye, L. C.; Zou, L.; Stamenkovic, I.; Kadoch, C.; Rivera, M. N. Cancer-Specific Retargeting of BAF Complexes by a Prion-like Domain. *Cell* **2017**, *171* (1), 163−178.
(19) Wegmann, S.; Eftekharzadeh, B.; Tepper, K.; Zoltowska, K. M.; Bennett, R. E.; Dujardin, S.; Laskowski, P. R.; MacKenzie, D.; Kamath, T.; Commins, C.; Vanderburg, C.; Roe, A. D.; Fan, Z. Y.; Molliex, A. M.; Hernandez-Vega, A.; Muller, D.; Hyman, A. A.; Mandelkow, E.; Taylor, J. P.; Hyman, B. T. Tau Protein Liquid-Liquid Phase Separation Can Initiate Tau Aggregation. *EMBO J.* **2018**, *37* (7), No. e98049.
(20) Patel, A.; Lee, H. O.; Jawerth, L.; Maharana, S.; Jahnel, M.; Hein, M. Y.; Stoynov, S.; Mahamid, J.; Saha, S.; Franzmann, T. M.; Pozniakovski, A.; Poser, I.; Maghelli, N.; Royer, L. A.; Weigert, M.; Myers, E. W.; Grill, S.; Drechsel, D.; Hyman, A. A.; Alberti, S. A Liquid-to-Solid Phase Transition of the ALS Protein FUS Accelerated by Disease Mutation. *Cell* **2015**, *162* (5), 1066−1077.
(21) Li, P. L.; Banjade, S.; Cheng, H. C.; Kim, S.; Chen, B.; Guo, L.; Llaguno, M.; Hollingsworth, J. V.; King, D. S.; Banani, S. F.; Russo, P. S.; Jiang, Q. X.; Nixon, B. T.; Rosen, M. K. Phase Transitions in The Assembly of Multivalent Signalling Proteins. *Nature* **2012**, *483* (7389), 336−340.
(22) Dyson, H. J.; Wright, P. E. Intrinsically Unstructured Proteins and Their Functions. *Nat. Rev. Mol. Cell Biol.* **2005**, *6* (3), 197−208.
(23) Hofmann, H.; Soranno, A.; Borgia, A.; Gast, K.; Nettels, D.; Schuler, B. Polymer Scaling Laws of Unfolded and Intrinsically Disordered Proteins Quantified With Single-Molecule Spectroscopy. *Proc. Natl. Acad. Sci. U. S. A.* **2012**, *109* (40), 16155−16160.
(24) Davey, N. E.; Trave, G.; Gibson, T. J. How Viruses Hijack Cell Regulation. *Trends Biochem. Sci.* **2011**, *36* (3), 159−169.
(25) Novoa, R. R.; Calderita, G.; Arranz, R.; Fontana, J.; Granzow, H.; Risco, C. Virus Factories: Associations of Cell Organelles for Viral Replication and Morphogenesis. *Biol. Cell* **2005**, *97* (2), 147−172.
(26) Miller, S.; Krijnse-Locker, J. Modification of Intracellular Membrane Structures For Virus Replication. *Nat. Rev. Microbiol.* **2008**, *6* (5), 363−374.
(27) Moradpour, D.; Penin, F.; Rice, C. M. Replication of Hepatitis C Virus. *Nat. Rev. Microbiol.* **2007**, *5* (6), 453−463.
(28) Paul, D.; Bartenschlager, R. Flaviviridae Replication Organelles: Oh, What a Tangled Web We Weave. In *Annual Review of Virology*; Enquist, L. W., Ed.; Annual Reviews: Palo Alto, 2015; Vol. *2*, pp 289−310.
(29) Quinkert, D.; Bartenschlager, R.; Lohmann, V. Quantitative Analysis of the Hepatitis C Virus Replication Complex. *Journal of Virology* **2005**, *79* (21), 13594−13605.
(30) Lindenbach, B. D.; Rice, C. M. Unravelling Hepatitis C Virus Replication from Genome to Function. *Nature* **2005**, *436* (7053), 933−938.
(31) Gouttenoire, J.; Castet, V.; Montserret, R.; Arora, N.; Raussens, V.; Ruysschaert, J. M.; Diesis, E.; Blum, H. E.; Penin, F.; Moradpour, D. Identification of a Novel Determinant for Membrane Association in Hepatitis C Virus Nonstructural Protein 4B. *J. Virol.* **2009**, *83* (12), 6257−6268.
(32) Gouttenoire, J.; Penin, F.; Moradpour, D. Hepatitis C Virus Nonstructural Protein 4B a Journey into Unexplored Territory. *Rev. Med. Virol.* **2010**, *20* (2), 117−129.
(33) Drin, G.; Antonny, B. Amphipathic Helices and Membrane Curvature. *FEBS Lett.* **2010**, *584* (9), 1840−1847.
(34) Gouttenoire, J.; Roingeard, P.; Penin, F.; Moradpour, D. Amphipathic Alpha-Helix AH2 is a Major Determinant for the Oligomerization of Hepatitis C Virus Nonstructural Protein 4B. *J. Virol.* **2010**, *84* (24), 12529−12537.
(35) Schindelin, J.; Arganda-Carreras, I.; Frise, E.; Kaynig, V.; Longair, M.; Pietzsch, T.; Preibisch, S.; Rueden, C.; Saalfeld, S.; Schmid, B.; Tinevez, J.-Y.; White, D. J.; Hartenstein, V.; Eliceiri, K.; Tomancak, P.; Cardona, A. Fiji: An Open-Source Platform for Biological-Image Analysis. *Nat. Methods* **2012**, *9*, 676−682.

DOI: 10.1021/acs.biomac.9b00081
Biomacromolecules 2019, 20, 1709−1718

(36) Angelova, M. I.; Dimitrov, D. S. Liposome Electroformation. *Faraday Discuss. Chem. Soc.* **1986**, *81* (0), 303−311.
(37) Rapsomaniki, M. A.; Kotsantis, P.; Symeonidou, I.-E.; Giakoumakis, N.-N.; Taraviras, S.; Lygerou, Z. easyFRAP: An Interactive, Easy-To-Use Tool for Qualitative and Quantitative Analysis of FRAP Data. *Bioinformatics* **2012**, *28* (13), 1800−1801.
(38) Kang, M.; Day, C. A.; Kenworthy, A. K.; DiBenedetto, E. Simplified Equation to Extract Diffusion Coefficients from Confocal FRAP Data. *Traffic* **2012**, *13* (12), 1589−1600.
(39) Bhat, P. P.; Appathurai, S.; Harris, M. T.; Pasquali, M.; McKinley, G. H.; Basaran, O. A. Formation of Beads-On-A-String Structures during Break-Up of Viscoelastic Filaments. *Nat. Phys.* **2010**, *6* (8), 625−631.
(40) Kyoung, M.; Sheets, E. D. Vesicle Diffusion Close to a Membrane: Intermembrane Interactions Measured with Fluorescence Correlation Spectroscopy. *Biophys. J.* **2008**, *95* (12), 5789−5797.
(41) Cao, X.; Bansil, R.; Gantz, D.; Moore, E. W.; Niu, N.; Afdhal, N. H. Diffusion Behavior of Lipid Vesicles in Entangled Polymer Solutions. *Biophys. J.* **1997**, *73* (4), 1932−1939.
(42) Rusu, L.; Lumma, D.; Radler, J. O. Charge and Size Dependence of Liposome Diffusion in Semidilute Biopolymer Solutions. *Macromol. Biosci.* **2010**, *10* (12), 1465−1472.
(43) Cho, N. J.; Dvory-Sobol, H.; Lee, C.; Cho, S. J.; Bryson, P.; Masek, M.; Elazar, M.; Frank, C. W.; Glenn, J. S. Identification of a Class Of HCV Inhibitors Directed Against the Nonstructural Protein NS4B. *Sci. Transl. Med.* **2010**, *2* (15), 15ra6.
(44) Aizaki, H.; Lee, K. J.; Sung, V. M. H.; Ishiko, H.; Lai, M. M. C. Characterization of the Hepatitis C Virus RNA Replication Complex Associated with Lipid Rafts. *Virology* **2004**, *324* (2), 450−461.
(45) Aizaki, H.; Morikawa, K.; Fukasawa, M.; Hara, H.; Inoue, Y.; Tani, H.; Saito, K.; Nishijima, M.; Hanada, K.; Matsuura, Y.; Lai, M. A. C.; Miyamura, T.; Wakita, T.; Suzuki, T. Critical Role of Virion-Associated Cholesterol and Sphingolipid in Hepatitis C Virus Infection. *J. Virol.* **2008**, *82* (12), 5715−5724.
(46) Chen, D. T. N.; Wen, Q.; Janmey, P. A.; Crocker, J. C.; Yodh, A. G. Rheology of Soft Materials. In *Annual Review of Condensed Matter Physics*; Langer, J. S., Ed.; Annual Reviews: Palo Alto, 2010; Vol. *1*, pp 301−322.
(47) Krimm, S.; Bandekar, J. Vibrational Spectroscopy and Conformation of Peptides, Polypeptides, and Proteins. *Adv. Protein Chem.* **1986**, *38*, 181−364.
(48) Snyder, R. G.; Strauss, H. L.; Elliger, C. A. C-H Stretching Modes and the Structure of Normal-Alkyl Chains. 1. Long, Disordered Chains. *J. Phys. Chem.* **1982**, *86* (26), 5145−5150.
(49) Barth, A. Infrared Spectroscopy of Proteins. *Biochim. Biophys. Acta, Bioenerg.* **2007**, *1767* (9), 1073−1101.
(50) Rothschild, K. J.; Clark, N. A. Polarized Infrared Spectroscopy of Oriented Purple Membrane. *Biophys. J.* **1979**, *25* (3), 473−487.
(51) Rothschild, K. J.; Sanches, R.; Hsiao, T. L.; Clark, N. A. A Spectroscopic Study of Rhodopsin Alpha-Helix Orientation. *Biophys. J.* **1980**, *31* (1), 53−64.
(52) Goormaghtigh, E.; Cabiaux, V.; Ruysschaert, J. M. Determination of Soluble and Membrane Protein Structure by Fourier Transform Infrared Spectroscopy. II. Experimental Aspects, Side Chain Structure, and H/D Exchange. *Subcell. Biochem.* **1994**, *23*, 363−403.
(53) Ladokhin, A. S.; Jayasinghe, S.; White, S. H. How to Measure and Analyze Tryptophan Fluorescence in Membranes Properly, and Why Bother? *Anal. Biochem.* **2000**, *285* (2), 235−245.
(54) Briggs, E. L. A.; Gomes, R. G. B.; Elhussein, M.; Collier, W.; Findlow, I. S.; Khalid, S.; McCormick, C. J.; Williamson, P. T. F. Interaction Between the NS4B Amphipathic Helix, AH2, and Charged Lipid Headgroups Alters Membrane Morphology and AH2 Oligomeric State - Implications For The Hepatitis C Virus Life Cycle. *Biochim. Biophys. Acta, Biomembr.* **2015**, *1848* (8), 1671−1677.
(55) Wang, Y.; Wang, Y.; Breed, D. R.; Manoharan, V. N.; Feng, L.; Hollingsworth, A. D.; Weck, M.; Pine, D. J. Colloids with Valence and Specific Directional Bonding. *Nature* **2012**, *491*, 51−55.

DOI: 10.1021/acs.biomac.9b00081
Biomacromolecules 2019, 20, 1709−1718